

Proceedings of the ASME 2013 Conference on Smart Materials, Adaptive Structures and Intelligent Systems
SMASIS2013

September 16-18, 2013, Snowbird, Utah, USA

SMASIS2013-3031

DESIGN OPTIMIZATION OF A TWIST COMPLIANT MECHANISM WITH NONLINEAR STIFFNESS

Yashwanth Tummala

Ph.D. Candidate
Dept. of Mechanical and Nuclear Engineering
The Pennsylvania State University
University Park, PA, USA

Aimy Wissa

Ph.D. Candidate
Dept. of Aerospace Engineering
University of Maryland
National Institute of Aerospace
Hampton, VA, USA

Mary Frecker

Professor
Dept. of Mechanical and Nuclear Engineering
The Pennsylvania State University
University Park, PA, USA

James E. Hubbard Jr.

Langley Distinguished Professor Dept. of Aerospace Engineering University of Maryland National Institute of Aerospace Hampton, VA, USA

ABSTRACT

A contact aided compliant mechanism called twist compliant mechanism is presented in this paper. This mechanism has nonlinear stiffness when it is twisted in both directions along its axis. The inner core of the mechanism is responsible for its flexibility in one twisting direction. The contact surfaces of the cross-members and compliant sectors are responsible for its high stiffness in the opposite direction. A twist compliant mechanism with desired twist angle and stiffness can be designed by choosing the right thickness of its cross-members, thickness of the core and thickness of its sectors. A multi-objective optimization problem with three objective functions is proposed in this paper, and used to design an optimal twist compliant mechanism with desired deflection. The objective functions are to minimize the mass and maximum von Mises stress observed, while minimizing or maximizing the twist angles under specific loading conditions. The multi-objective optimization problem proposed in this paper is solved using an ornithopter flight research platform as a case study, with the goal of using the twist compliant mechanism to achieve passive twisting of the wing during upstroke, while keeping the wing fully extended and rigid during the downstroke. Prototype twist compliant mechanisms have been fabricated using a waterjet cutter and will be tested as part of future work.

. NOMENCLATURE

α = Parameter to determine cutoff stress in the optimization

 λ = Binary variable

 ρ_{delrin} = Density of DelrinTM (kg/m³)

 σ_{cutoff} = Stress limit on TCM designs used during TCM

optimization (Pa)

 σ_{max} = Maximum von Mises stress in a TCM (Pa)

 $\sigma_{penalty}$ = Penalty value for stress objective function (Pa)

 σ_{vield} = Yield stress of TCM material (Pa)

 Ψ_{max} = Maximum twist angle observed in a TCM (rad)

 $\Psi_{penalty}$ = Penalty value for twist angle objective function

(rad)

 f_I = Mass objective function in TCM optimization

 f_2 = Twist angle objective function in TCM

optimization

 f_3 = Stress objective function in TCM optimization $lb_{c in}$ = Lower bound on the inner radius of the core $lb_{c out}$ = Lower bound on the outer radius of the core

 lb_{fin} = Lower bound on the inner radius of the sector lb_{fout} = Lower bound on the outer radius of the sector

 lb_t = Lower bound on the thickness of the cross-

members

 t_{cm} = Thickness of the cross-members

 $ub_{c in}$ = Upper bound on the inner radius of the core

 $ub_{c \ out}$ = Upper bound on the outer radius of the core $ub_{f \ in}$ = Upper bound on the inner radius of the sector $ub_{f \ out}$ = Upper bound on the outer radius of the sector ub_t = Upper bound on the thickness of the crossmembers

M = Mass of a TCM (kg)

 $M_{penalty}$ = Penalty value for mass objective function (kg)

Y = Direction along the length of a TCM

 R_{fin} = Inner radius of the sectors R_{fout} = Outer radius of the sectors

 L_t = Length of the twist compliant mechanism

 g_c = Contact gap

 $R_{c in}$ = Inner radius of the inner core $R_{c out}$ = Outer radius of the inner core

2. INTRODUCTION

Contact aided Compliant Mechanisms (CCMs) are a class of compliant mechanisms where the compliant members come into contact with one another to perform a specific task or to improve the performance of the mechanism itself. A wide variety of contact interactions have been considered ranging from a simple case involving single point contact to the more complex case of multiple contacts between different parts of the compliant mechanism itself. CCMs were first introduced in the literature by Mankame and Ananthasuresh in 2002 [1]. Such mechanisms can have nonlinear stiffness [2-4], provide stress relief [5-7] and can also generate a non-smooth path [1]. Reddy et. al. designed CCMs to trace large, non-smooth paths using topology optimization and finite element analysis (FEA) [8]. Mehta et. al. have designed honeycomb cells with contact elements called Contact Aided Cellular Compliant Mechanisms (C³Ms) to obtain stress relief [5]. Cirone et. al. have designed these C³Ms with curved walls for high strain applications [9]. Halverson et. al. have designed a bi-axial CCM for spinal arthroplasty [10]. Cannon and Howell have designed a contact aided compliant revolute joint [11]. While not a contact aided compliant mechanism, a unique revolute flexure joint called split-tube flexure that enables compliant mechanism designs with considerably larger range-of-motion than a conventional thin beam flexure has been designed by Goldfarb and Speich [12].

Lachenal et. al. have developed a multi-stable composite twisting structure for morphing applications [13]. This structure consists of two pre-stressed flat flanges connected by rigid spokes and has zero-stiffness along the axis of twist. Schultz has developed an air-foil like structure capable of twisting [14]. This structure consists of two curved shells that are joined to form an airfoil-like structure with two stable configurations. The structure is transformed between the stable states by a snap-through action which occurs because of the piezocomposite actuators. Hence this structure is active in nature. Many other researchers have also developed active composite structures to achieve twisting. One such recent

effort is by Palmre et. al. where they have developed a IPMC-enabled bio-inspired bending/twisting fin for underwater applications[15].

The twist compliant mechanism presented in this paper is a contact aided compliant mechanism that is passive in nature. This mechanism is designed to have nonlinear stiffness in the twisting direction. When it is twisted along its length, it is flexible in one direction but is stiff when twisted in the other direction. Such a mechanism is useful to achieve passive twisting in the wings of an avian-scale ornithopter. Ornithopters, or flapping wing Unmanned Aerial Vehicles (UAVs), have the potential to revolutionize UAV performance in both the civil and military sectors [16]. Our work aims at improving the performance of avian-scale ornithopters during steady level flight by integrating passive compliant mechanisms into the wing structure. Previous work by the authors has shown that such an approach is feasible and that implementation of a single degree of freedom (DOF) bending compliant mechanism resulted in significant improvements in the performance of a test ornithopter [4, 17]. To achieve an avian-inspired wing gait in the ornithopter, the outer section of the wing must bend, sweep and twist simultaneously during the upstroke, while remaining fully extended during the downstroke [17]. We have also presented an approach to achieve simultaneous bending and sweep using a single passive compliant mechanism [18, 19]. A novel aspect of our approach is that the compliant mechanisms are completely passive, i.e., they deform as a natural consequence of the aerodynamic loads encountered during flight. There are no additional actuators or sensors required.

The reminder of this paper is organized as follows. Section 3 introduces the concept of the twist compliant mechanism (TCM), its geometric parameters and nonlinear stiffness properties. Section 4 presents a multi-objective design optimization problem formulated to optimize the TCM. The TCM optimization problem was then solved for the ornithopter application and the results are presented in section 5. Finally, section 6 includes the conclusions and future work.

3. TWIST COMPLIANT MECHANISM

The twist compliant mechanism (TCM), shown in Figure 1, is a novel contact aided compliant mechanism with nonlinear stiffness properties. Parts of this compliant mechanism are the inner core, cross-members and compliant sectors (shown in Figure 1). There are four sectors in the mechanism shown in Figure 1. This mechanism is designed to be flexible when it is twisted in the counter-clockwise direction. The torsional stiffness of the mechanism in the counter-clockwise direction is primarily due to the inner core (Figure 2(a)). When this mechanism is twisted in the clockwise direction, the sectors come into contact (Figure 2(b)) thus increasing its torsional stiffness. The nonlinear stiffness of a typical TCM is shown in Figure 3. The plot shown was generated by using ANSYS (FEA software)

accounting for contact at the surfaces of the sectors. The loading conditions that were used to generate the plot are shown in Figure 1(b).

A TCM with a desired twist angle and desired stiffness can be designed by choosing the right geometric parameters that define its design (Figure 4). The geometric parameters that affect the stiffness of this compliant mechanism are the length of the TCM L_t , number of sectors n, contact gap g_c (dotted black arrows), thickness of the cross-members t_{cm} (blue arrows), inner radius of the inner core $R_{c in}$ (red arrow), outer radius of the inner core $R_{c out}$ (dashed red arrow), inner radius of the sectors $R_{f in}$ (dashed black arrow), and outer radius of the sectors $R_{f out}$ (black arrow). A design optimization procedure is necessary in order to determine the optimal TCM a specific application. Hence a multi-objective optimization problem was formulated as part of the design optimization procedure and is presented in the next section.

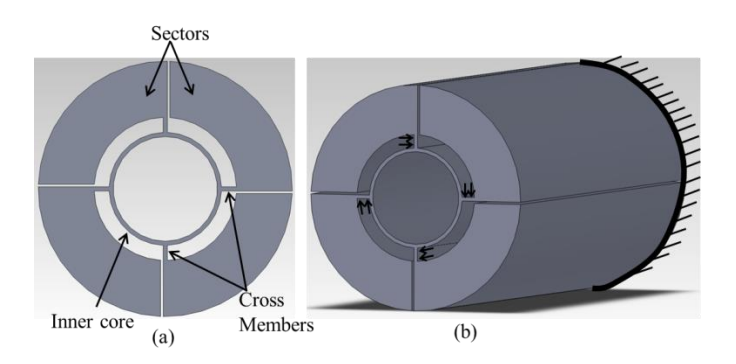


Figure 1 Twist compliant mechanism. (a) Cross-section (b) Loading conditions.

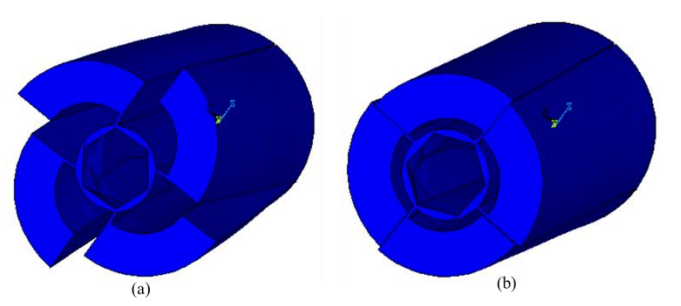


Figure 2 Twisting of TCM in (a) counter-clockwise direction (b) clockwise direction.

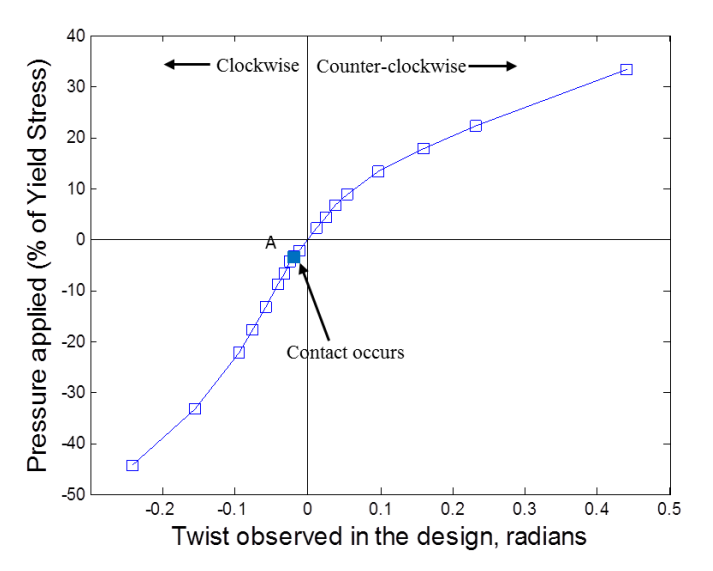


Figure 3 The twist compliant mechanism exhibits nonlinear stiffness.

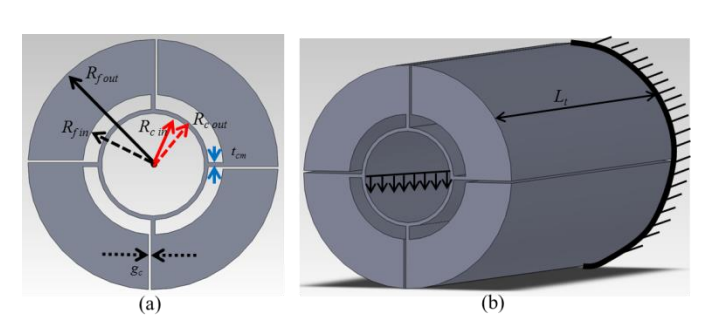


Figure 4 (a) Geometric parameters that affect the stiffness of the twist compliant mechanism. (b) Loading conditions used during the design optimization.

DESIGN OPTIMIZATION

There are eight geometric parameters that define the stiffness of a TCM. Among these parameters, the length of the TCM L_t , number of sectors n, contact gap g_c are fixed to simplify the design optimization procedure. To determine the optimal cross-section of the TCM and the geometric parameters associated with the cross-section (t_{cm} , $R_{c in}$, $R_{c out}$, $R_{f in}$, $R_{f out}$) a multi-objective optimization problem with three objectives is formulated. The optimization problem is defined by Equations 1-16 and is solved using a genetic algorithm.

> Minimize (f_1, f_3) Maximize (f_2)

S.T.

$$R_{fin} - R_{fout} < 0 (1)$$

$$R_{c in} - R_{c out} < 0$$
 (2)
 $R_{c out} - R_{f in} < 0$ (3)
 $lb_{f in} \le R_{f in} \le ub_{f in}$ (4)

$$R_{cout} - R_{fin} < 0 (3)$$

$$lb_{fin} < R_{fin} < ub_{fin} \tag{4}$$

$$lb_{fout} \le R_{fout} \le ub_{fout} \tag{5}$$

$$lb_{c in} \leq R_{c in} \leq ub_{c in} \tag{6}$$

$$lb_{c out} \le R_{c out} \le ub_{c out} \tag{7}$$

$$lb_t \le t_{cm} \le ub_t \tag{8}$$

Where,

$$f_1 = \lambda * M + (1 - \lambda) * M_{penalty}$$
 (9)

$$f_2 = \lambda * \Psi_{max} - (1 - \lambda) * \Psi_{penalty}$$
 (10)

$$f_3 = \lambda * \sigma_{max} + (1 - \lambda) * \sigma_{penalty}$$
 (11)

$$\lambda = \begin{cases} 1 & \text{if } \sigma_{max} \leq \sigma_{cutoff} \\ 0 & \text{if } \sigma_{max} > \sigma_{cutoff} \end{cases}$$
 (12)

$$\sigma_{cutoff} = \alpha * \sigma_{vield} \tag{13}$$

$$M_{penalty} \gg M$$
 (14)

$$\Psi_{nenalty} \ll \Psi_{max}$$
 (15)

$$\sigma_{penalty} \gg \sigma_{max}$$
 (16)

The constraints given by Equations 1-3 ensure that geometrically feasible TCM cross-sections are generated. The inequality constraint in Equation 1 ensures that the outer radius of the sector is greater than the inner radius of the sector. The inequality constraint in Equation 2 ensures that outer radius of the inner core is greater than the inner radius of the inner core. The inequality constraint in Equation 3 ensures that the inner radius of the sector is greater than the outer radius of the inner core and hence also ensures that the crossmembers are of finite length. The inequalities in Equations 4-8 define the lower and upper bounds on the five geometric parameters. The objective functions f_1 , f_2 , and f_3 given by Equations 9, 10, and 11 respectively are calculated using a commercial finite element package, ANSYS. Objective function f_1 is the mass, f_2 is the twist angle, and f_3 is the maximum von Mises stress of a TCM.

Constraints on the objective functions were imposed using the penalty values, $M_{penalty}$, $\Psi_{penalty}$, $\sigma_{penalty}$, and the binary variable λ . These penalty values (Equations 14, 15, and 16) were chosen such that an infeasible design, determined by Equation 12, was assigned a poor value of the objective function; such designs are terminated and not allowed to propagate into future generations. Computational time is also an important factor in this optimization because finite element analysis is being performed on each of the TCM designs in each generation. Taking the computational resources and complexity of the problem into consideration, penalty values have proven to be very effective in driving the optimization towards feasible regions in the design space. A TCM design is considered to be infeasible if the maximum von Mises stress in the design, σ_{max} , is greater than a cutoff stress limit, σ_{cutoff} , calculated from Equation 13. This limit is selected by the designer by choosing an appropriate value for α , which can be a function of the safety factor for a material with yield stress, σ_{yield} .

An effective approach to solving the optimization problem is to use heuristic optimization algorithms like Multi-Objective Evolutionary Algorithms (MOEAs). Zhou et al. [20] present a survey of the state of the art MOEAs. A controlled elitist genetic algorithm which is a variant of NSGA-II [21, 22] was used for the optimization. This genetic algorithm is part of the optimization toolbox provided in MATLAB. The optimization problem was implemented in an algorithm shown in the schematic in Figure 5. Convergence of a multi-objective optimization problem can be determined with the help of various convergence metrics such as that proposed by Deb and Jain [23]. Deb's metric is widely used in the field of MOEAs to test convergence. This metric is a measure of the average distance between the reference set and the non-dominated population members of each of the generations; this average distance is normalized to always lie between 0 and 1. The optimization algorithm shown is determined to have converged when the actual average distance is less than 0.06.

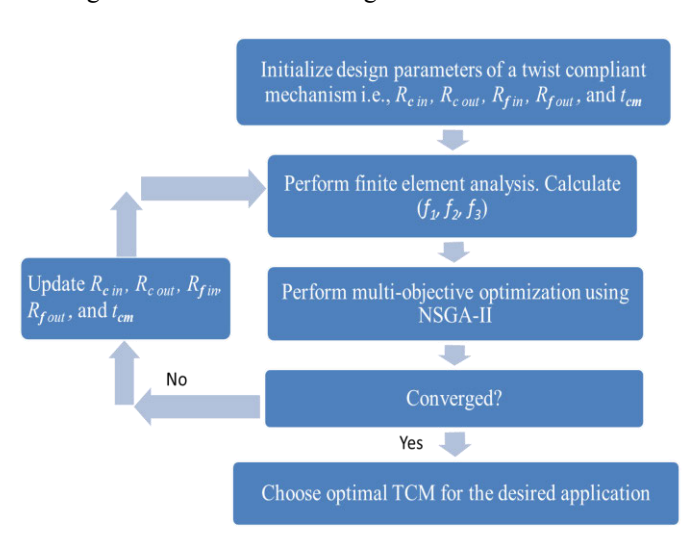


Figure 5 Schematic representation of the design optimization procedure for TCM design.

The design optimization procedure is implemented as a case study to design a twist compliant mechanism for passive twisting of ornithopter wings. Details and results are presented in the next section.

5. CASE STUDY

The design optimization procedure is implemented to design a twist compliant mechanism for passive twisting of an ornithopter's wings during steady level flight. Because of its nonlinear stiffness properties the twist compliant mechanism is expected to experience passive twisting during upstroke. During downstroke, because of the sectors coming into

contact, the wings are expected to stay fully extended and rigid. In either direction, the twist occurs as a natural consequence of the aerodynamic loads encountered during flight.

This twist compliant mechanism for the ornithopter application is assumed to be inserted in the leading edge wing spar and rigidly connected to the diagonal spar. To perform the design optimization procedure on the twist compliant mechanisms, an estimate of the twisting moment acting on the TCM is necessary. This twisting moment is calculated based on the integrated lift, center of pressure and the mean quarterchord length. To estimate the aerodynamic loads acting on the ornithopter wing structure, the authors conducted flapping experiments using an ornithopter equipped with strain gauges to measure the deformation of the leading edge spar [17]. Based on the results of these experiments, the integrated peak lift load was estimated to be about 10 N. The test ornithopter has a wing span of 1.06 m and a mean chord of 0.21 m. It is assumed here that the lift load acts on the wing at the center of pressure and that center of pressure is at the mean quarter chord from the leading edge spar (Figure 6). Based on these assumptions, the maximum twisting moment that can be seen at the leading edge spar is 0.525 Nm. This value of the twisting moment was used during the design optimization procedure of the twist compliant mechanisms. The twisting moment is applied as a distributed load along the length of the TCM on the inner surface of the inner core as shown in Figure 4(b). The net twisting moment acting at the root of the TCM, because of this distributed load, is 0.525 Nm. A counterclockwise twisting moment is applied on the TCM to simulate the upstroke condition and a clockwise twisting moment is applied on the TCM to simulate the downstroke condition. The boundary conditions used during the finite element analysis of TCMs are also shown in the same figure.

This ornithopter application imposes dimensional constraints on the TCM designs as it is based on the actual test platform. The cross-section of the TCM should fit into a square with a 12.7 mm side. For application purposes, the length (L_t) of all the TCMs are fixed to be 25.4 mm long and the contact gap (g_c) was fixed to be 300 μ m.

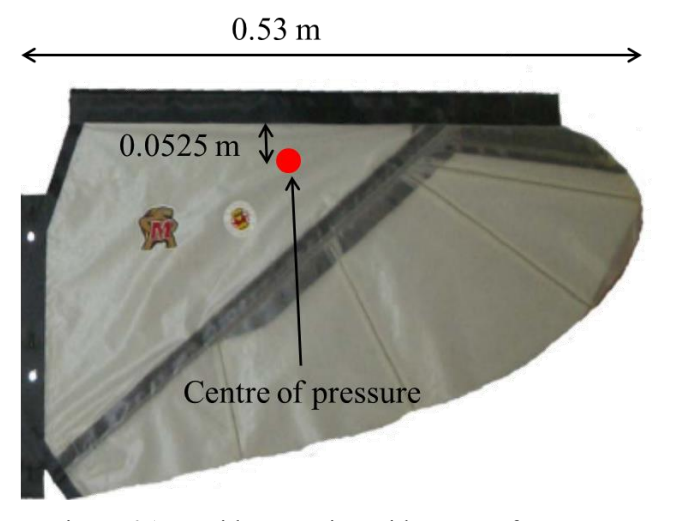


Figure 6 An ornithopter wing with centre of pressure.

Two types of finite element analyses were considered in the optimization. Since the application is dynamic in nature, dynamic finite element analysis was performed on the TCMs during optimization; however, the finite element package, ANSYS, can only perform linear analysis in this case. In reality, since the TCMs are going to be fabricated using DelrinTM (Dupont polymer), large deformations, nonlinear material properties and contact constraints must be incorporated in the finite element analysis. Hence an optimization using quasi-static analysis which can account for large deformation, nonlinear material properties and contact, was also performed. During the finite element analysis, Solid95, Conta174, Targe170, finite elements, and multi-linear material properties of DelrinTM were used [24, 25]. To understand the effects of number of sectors, TCMs with three, four, and five sectors were optimized using steady-state dynamic analysis during upstroke. Optimization of TCMs with three sectors using quasi-static analysis was also performed during both upstroke and downstroke to incorporate nonlinear material properties, large deformations, and contact. All of these cases are summarized in Table 1. The upper and lower bounds on the design variables that were used during the optimization are presented in Table 2. The lower bounds on the radii were determined based on the diameter of the leading edge spar while the upper bounds on the radii were determined based on the dimensional constraints imposed by the ornithopter application. All other parameters that were used during the optimization are shown in Table 3. When considering the upstroke condition, the twist angle objective function is maximized, while during downstroke the twist angle objective function is minimized. When minimizing the twist angle, the objective function Equation 15 changes to Equation 17. The results of the optimization procedure for all the cases listed in Table 1 are presented in the following subsection.

$$\Psi_{penalty} \gg \Psi_{max}$$
 (17)

Table 1 Different simulation cases that were considered during design optimization of TCM.

Type of Simulation	Upstroke/ Downstroke	n (Number of sectors)
Dynamic	Upstroke	3
Dynamic	Upstroke	4
Dynamic	Upstroke	5
Quasi-static	Upstroke	3
Quasi-static	Downstroke	3

Table 2 Upper and lower bounds on the geometric parameters used during design optimization of TCM.

Design Parameters	R _{c in} (m)	$R_{c out}$ (m)	R_{fin} (m)	R _{f out} (m)	t_{cm} (m)
Lower Bound	0.0025	0.0025	0.0025	0.0025	0.0003
Upper Bound	0.006	0.006	0.006	0.0064	0.002

Table 3 Other parameters used during design optimization of TCM.

Variable	Value		
α	1		
$\sigma_{_{yield}}$	45*10 ⁶ Pa		
$M_{\it penalty}$	14.2*10 ⁶ kg		
$\Psi_{penalty}$	1000		
$\sigma_{penalty}$	10000 * 10 ⁶ Pa		
Population size	100		
$ ho_{_{delrin}}$	1420 kg/m ³		

5.1. Optimization Results

For the three objective functions in the design optimization procedure the optimal designs comprise a 3-D Pareto front. It is difficult to visualize the results in 3-D, however. Hence, the twist angle and normalized maximum von-Mises stress objectives will be compared in a 2-D plot, while the normalized mass of the TCM is represented by the size of the marker. Figure 7 presents the optimization results of steady-state dynamic analysis performed on three, four, and five sector TCMs. Some of the sample cross-sections are also shown here. Figure 8 presents the results of quasi-static optimization procedure performed on the three sector TCMs for upstroke. Figure 9 presents the results of quasi-static optimization procedure performed on three sector TCMs for downstroke. Sample cross-sections of the optimal TCMs are

also shown in each of these plots. These results are discussed in the following sub-section.

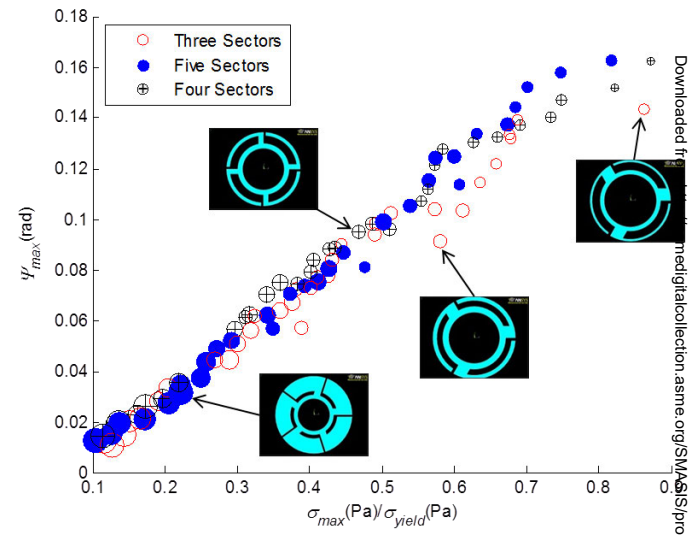


Figure 7 Dynamic optimization results for three, four, and five sector designs. Marker size represents the relative mass of each of the designs.

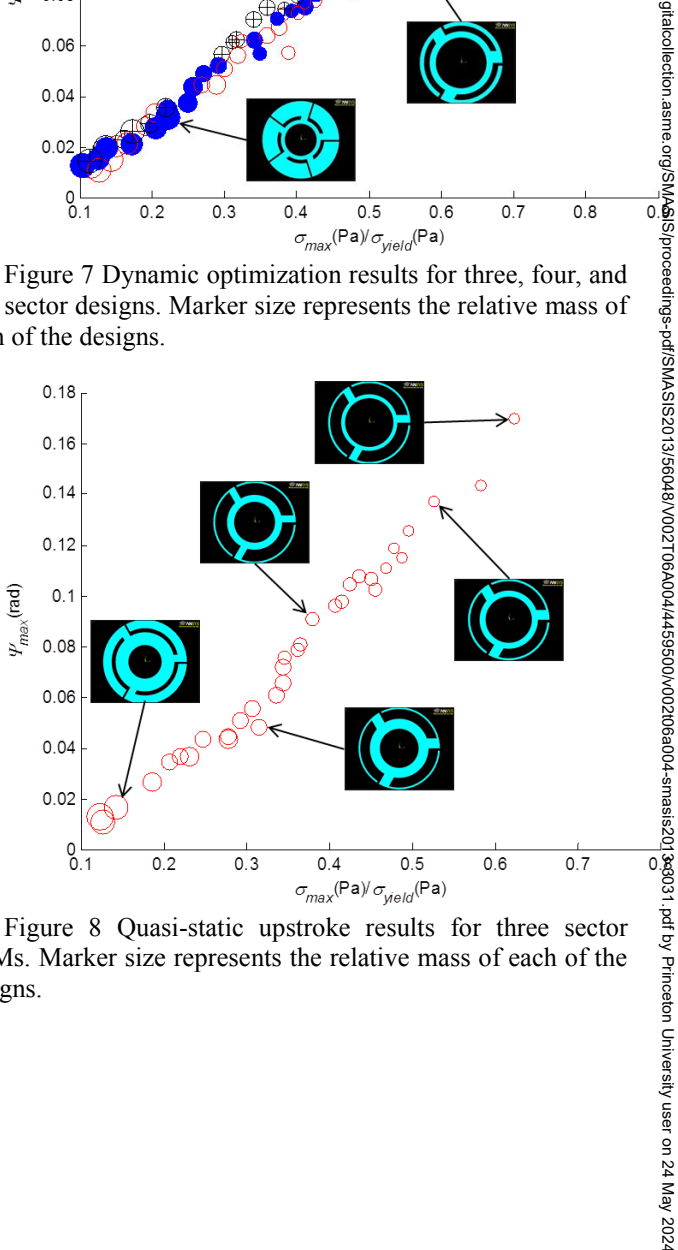


Figure 8 Quasi-static upstroke results for three sector TCMs. Marker size represents the relative mass of each of the designs.

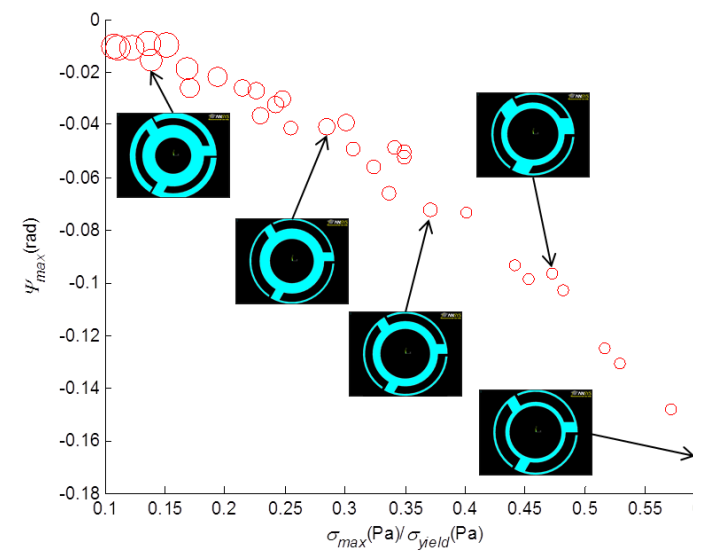


Figure 9 Quasi-static downstroke results for three sector TCMs. Marker size represents the relative mass of each of the designs.

5.2. Discussion

Figure 7 shows the upstroke optimization results of three, four, and five sector TCMs using steady-state dynamic analysis. The objectives were to maximize the twist angle during upstroke while minimizing the maximum von-Mises stress observed in the TCM designs. Hence the best design would be located in the upper left corner of the plot. A designer can choose an optimal design from the Pareto front based on the desired stress limit and the required twist angle. It can be seen in the plot that the markers close to the origin are larger in size than the markers that are farther away suggesting that designs that are close the origin have more mass. One such design that is close to the origin is shown in the plot. This design has a higher second moment of inertia about its length axis than the other designs. Note that as the second moment of inertia of a TCM's cross-section about the length axis increases, its mass and torsional stiffness increases. This is because the second moment of inertia is proportional to the area of the cross-section. Such an increase in the inertia causes a decrease in the twist angle and hence a decrease in the maximum von-Mises stress observed in the TCM. Hence the designs close to the origin have higher mass, higher second moment of inertia about the length axis and lower deflections compared to the other members of the Pareto front that are farther away from the origin. Figure 7 also suggests that increasing the number of sectors in a TCM does not necessarily cause any changes in the performance of TCM. Hence a designer can choose the TCM with three sectors without any loss in the performance.

For the ornithopter application during downstroke, the twist compliant mechanism is expected to have minimum possible twist angle. Since increasing the number of sectors also increases the number of contact gaps, the designer should choose minimum possible number of sectors in order to minimize the downstroke deflection in the twist compliant mechanism. Based on the Pareto optimal front, it can also be inferred that the thickness of the sectors decreases as the twisting deflection of the designs increases.

Figure 8 presents the quasi-static optimization results of the design optimization procedure on a three sector TCM for upstroke. These results also suggest that mass of the TCMs close to the origin is higher because they have higher second moment of inertia about their length axis, and hence have lower von-Mises stress and twist angle. The range of twist angle is about the same as the Pareto front obtained from the dynamic analysis also suggesting that TCMs with four or five sectors do not provide any benefit. The thickness of the sectors decreases as the twist angle of the design increases.

Figure 9 presents the quasi-static design optimization results of three sector TCMs for the downstroke condition. During downstroke the loads applied are in the clockwise direction. As a result, twisting occurs in the clockwise direction and hence the Y-axis in the plot has negative twist angles. The objectives are to minimize the twist angle, mass, and maximum von-Mises stress observed. Optimal TCMs are located in the top left corner of the plot. The relative mass of each of the designs are again represented by the size of the marker. It can be observed from the plot that designs located close to the origin have higher mass than the designs that are farther away. This again suggests that these designs have higher second moment of inertia about their length axis and hence smaller twist angle.

Hence the upstroke and downstroke requirements for the TCM in an ornithopter application are conflicting in nature. For the upstroke, the TCM is expected to have smaller second moment of inertia because twist angle needs to be maximized. On the other hand, during downstroke, minimum possible twist angle is required and hence the second moment of inertia of a TCM needs to be high. This warrants the need for a design optimization procedure to determine the optimal TCM for a specific application. Since both the desired upstroke and downstroke twist angles cannot be met simultaneously, a designer will have to first prioritize the upstroke or downstroke twist angle. For the ornithopter application, upstroke twist angle is important and hence a design from Figure 7 which satisfies the minimum twist angle requirement subject to the stress limit will be chosen for testing purposes.

6. CONCLUSIONS & FUTURE WORK

A novel contact aided compliant mechanism with nonlinear stiffness properties called twist compliant mechanism is presented. This mechanism is designed to achieve passive twisting of ornithopter wings. A design optimization procedure with a multi-objective optimization problem was developed to design and optimize the twist compliant mechanisms. As a case study, design optimization

was performed on the TCMs to design a twist compliant mechanism for ornithopter application. Based on the case study, it can be concluded that the number of sectors in a TCM has little effect on its performance during upstroke. Also, as the second moment of inertia of the cross-section of a TCM about its length axis increases, its mass and stiffness increases. As a result the twist angle is small and the associated von-Mises stress is also small. For upstroke, the second moment of inertia has to be very small to achieve maximum possible twist angle but for downstroke, the second moment of inertia has to be very high to achieve minimum possible twist angle. Based on the desired twist angle goals, an optimal TCM can be chosen from the optimal Pareto fronts. As part of the future work, these designs will be experimentally tested to validate the models and to demonstrate passive twisting of ornithopter wings.

7. ACKNOWLEDGEMENTS

The authors gratefully acknowledge the support of AFOSR grants FA9550-09-1-0632 and FA9550-13-0126 under the direction of Dr. David Stargel. The computational work was supported in part through instrumentation funded by the National Science Foundation through grant OCI–0821527. The resources of the NASA Langley Research Center, Pennsylvania State University, the University of Maryland and the Morpheus Lab are also appreciated.

8. REFERENCES

- 1. Mankame, N.D. and G.K. Ananthasuresh. Contact aided compliant mechanisms: Concept and preliminaries. in International Design Engineering Technical Conferences and Computers and Information in Engineering Conference. 2002. Montreal, QC, Canada: Web Portal ASME
- 2. Tummala, Y., Wissa, A., Frecker, M., Hubbard Jr., J. E. Design of a Passively Morphing Ornithopter Wing Using a Novel Compliant Spine. in Proceedings of Smart Materials, Adaptive Structures and Intelligent Systems Conference. 2010. Philadelphia, PA, United States.
- 3. Tummala, Y., Wissa, A., Frecker, M., Hubbard Jr., J. E. Design Optimization of a Compliant Spine for Dynamic Applications. in Proceedings of Smart Materials, Adaptive Structures and Intelligent Systems Conference. 2011. Scottsdale, AZ, United States.
- 4. Wissa, A., Tummala, Y., Hubbard Jr., J. E., and Frecker, M., *Passively Morphing Ornithopter Wings using a Novel Compliant Spine: Design and Testing.* Smart Materials and Structures, 2012. **21**(9).

- 5. Mehta, V., M. Frecker, and G.A. Lesieutre, *Stress relief in contact-aided compliant cellular mechanisms*. Journal of Mechanical Design, 2009. **131**: p. 0910091-09100911.
- 6. Mehta, V., M. Frecker, and G. Lesieutre. Contactaided compliant mechanisms for morphing aircraft skin. in Modeling, Signal Processing, and Control for Smart Structures 2008. 2008. USA: SPIE The International Society for Optical Engineering.
- 7. Mehta, V., M. Frecker, and G.A. Lesieutre, *Two-step design of multicontact-aided cellular compliant mechanisms for stress relief.* Journal of Mechanical Design, Transactions of the ASME, 2012. **134**(12).
- 8. Reddy, B.V.S.N., S.V. Naik, and A. Saxena, *Systematic Synthesis of Large Displacement Contact-Aided Monolithic Compliant Mechanisms*. Journal of Mechanical Design, 2012. **134**(1): p. 011007-12.
- 9. Cirone, S.A., et al., *Design of contact-aided compliant cellular mechanisms with curved walls*. Journal of Intelligent Material Systems and Structures, 2012. **23**(16): p. 1773-1785.
- 10. Halverson, P.A., L.L. Howell, and A.E. Bowden. A flexure-based bi-axial contact-aided compliant mechanism for spinal arthroplasty. in International Design Engineering Technical Conferences & Computers and Information in Engineering Conference. 2008. Brooklyn, New York.
- 11. Cannon, J.R. and L.L. Howell, *A compliant contact-aided revolute joint*. Mechanism and Machine Theory, 2005. **40**(11): p. 1273-1293.
- 12. Goldfarb, M. and J.E. Speich, *Well-behaved revolute flexure joint for compliant mechanism design*. Journal of Mechanical Design, Transactions of the ASME, 1999. **121**(3): p. 424-429.
- 13. Lachenal, X., P.M. Weaver, and S. Daynes. *Multistable composite twisting structure for morphing applications*. in *Proceedings of the Royal Society A: Mathematical, Physical and Engineering Sciences*. 2012. London, United Kingdom: Royal Society of London.
- 14. Schultz, M.R., *A concept for airfoil-like active bistable twisting structures*. Journal of Intelligent Material Systems and Structures, 2008. **19**(2): p. 157-169.
- 15. Palmre, V., et al., An IPMC-enabled bio-inspired bending/twisting fin for underwater applications. Smart Materials and Structures, 2013. **22**(1).
- 16. Shyy, W., M. Berg, and D. Ljungqvist, *Flapping and Flexible Wings for Biological and Micro Air Vehicles*. Progress in Aerospace Sciences, 1999. **35**(5): p. 455-505.
- 17. Wissa, A., Tummala, Y., Hubbard Jr., J. E., Frecker, M. *Testing of Novel Compliant Spines for Passive*

- Wing Morphing. in Proceedings of Smart Materials, Adaptive Structures and Intelligent Systems Conference. 2011. Scottsdale, AZ, United States.
- 18. Tummala, Y., Frecker, M., Wissa, A., Hubbard Jr., J. E. Design of Bend-and-Sweep Compliant Mechanism for Passive Shape Change. in Proceedings of Smart Materials, Adaptive Structures and Intelligent Systems Conference. 2012. Stone Mountain, GA, United States.
- 19. Tummala, Y., Frecker, M., Wissa, A., Hubbard Jr., J. E. Design and Optimization of a Bend-and-Sweep Compliant Mechanism. in International Design Engineering Technical Conferences & Computers and Information in Engineering Conference. 2013. Portland, Oregon
- 20. Zhou, A., Qu, Bo-Yang, Li, H., Zhao, Shi-Zheng, Suganthan, P. N. and Q. Zhang, *Multiobjective Evolutionary Algorithms: A Survey of the State of the Art.* Swarm and Evolutionary Computation, 2011. 1: p. 32-49.
- 21. Deb, K., et al., *A Fast and Elitist Multiobjective Genetic Algorithm: NSGA-II.* IEEE Transactions on Evolutionary Computation, 2002. **6**(2): p. 182-197.
- 22. Deb, K., *Multi-Objective Optimization Using Evolutionary Algorithms*. 2001, Chichester; New York: John Wiley & Sons.
- 23. Deb, K., Jain, S., Running Performance Metrics for Evolutionary Multi-Objective Optimization," in Technical Report KanGAL 2002004. 2002: Indian Institute of Technology Kanpur, India.
- 24. Dupont,

 <u>http://plastics.dupont.com/plastics/pdflit/americas/delrin/230323c.pdf</u>"2011.
- 25. Olympio, K.R., *Design of A Passive Flexible Skin for Morphing Aircraft Structures*," in *M.S. thesis*. 2006, The Pennsylvania State University.